

# Experimental digital quantum simulation of quantum tunneling

Guan Ru Feng<sup>1,2,\*</sup>, Yao Lu<sup>1,2\*</sup>, Liang Hao<sup>1,2</sup>, Fei Hao Zhang<sup>3</sup> and Gui Lu Long<sup>1,2†</sup>

<sup>1</sup>*State Key Laboratory of Low-dimensional Quantum Physics and Department of Physics, Tsinghua University, Beijing 100084, P. R. China*

<sup>2</sup>*Tsinghua National Laboratory for Information Science and Technology, Beijing 100084, P. R. China*

<sup>3</sup>*Department of Physics, Shandong Normal University, Jinan 250358, P. R. China*

(Dated: March 3, 2013)

It is well known that quantum computers are superior to classical computers in efficiently simulating quantum systems. Here we report the first experimental simulation of quantum tunneling through potential barriers, a widespread phenomenon of a unique quantum feature, via NMR techniques. Our experiment is based on the digital simulation algorithm that discretizes continuous space and time into lattices, and requires only two spin-1/2 nuclei without the need of ancillary qubits. The occurrence of quantum tunneling through a barrier is clearly observed through the experimental results. This experiment has clearly demonstrated the viability of quantum simulations for a wide range of quantum phenomena with not only discrete, but also continuous degrees of freedom.

PACS numbers: 03.65.Xp, 03.67.Ac, 03.67.Lx, 07.57.Pt

Quantum computation has become a subject of intense investigation since Feynman discussed the likelihood of simulating one quantum system by another [1]. Recent years have witnessed fruitful results in the development of quantum computation. Not only has Feynman's conjecture been confirmed, but it has also been demonstrated that quantum computers can solve problems, such as Shor's quantum algorithm for integer factorization [2] and Grover's quantum search algorithm [3], with a level of efficiency beyond the capability of classical computers. As conjectured by Feynman, simulation of the dynamics of quantum systems is one of the most important aims of quantum computation. Quantum simulations, such as the simulation of a many-body interaction Hamiltonian [4–6], the dynamics of entanglement [7, 8], quantum phase transitions [9, 10], and the calculations of molecular properties [11, 12] have been demonstrated in experiments. Quantum simulations are especially attractive for providing an exponential improvement compared to classical computations, which makes it a promising candidate in the analysis of chemical reactions[13, 14].

As a unique fundamental concept in quantum mechanics, quantum tunneling plays an essential role in many quantum phenomena, such as the tunneling of superconducting Cooper pairs [15]. Additionally, its properties are widely applied in modern devices and modern experimental techniques, such as the tunnel diode [16], the scanning tunneling microscope [17] and so on. Quantum tunneling is of continuous interest. Sornborger [18] proposed a small-scale digital simulation algorithm for demonstrating a one-particle wave function tunneling in a double-well potential using a quantum information pro-

cessor. In this paper, we realized the algorithm via the room temperature liquid state NMR of two qubits. Using the digital simulation algorithm, the continuous process of one-dimensional tunneling of a particle through a potential barrier is clearly demonstrated. Our experiment has shown that with very few qubits, interesting tunneling dynamics is simulated with a gate count that is within reach of current quantum architectures.

In the digital quantum simulation [18–20], the one-dimensional wave function  $\psi(x, t)$  of a single particle moving in square-like potential with Schrödinger equation as:

$$i\frac{\partial}{\partial t}|\psi(x, t)\rangle = \left[\frac{\hat{P}^2}{2m} + V(\hat{X})\right]|\psi(x, t)\rangle, \quad (1)$$

where  $\hat{P}$  and  $\hat{X}$  are momentum and position operators, respectively. Throughout the text we set  $\hbar$  to be 1. In the Schrödinger picture the evolution of the wave function with time can be straightforwardly given as:

$$|\psi(x, t + \Delta t)\rangle = e^{-i\left[\frac{\hat{P}^2}{2m} + V(\hat{X})\right]\Delta t}|\psi(x, t)\rangle, \quad (2)$$

which can be further decomposed according to the Trotter formula [18, 19]:

$$|\psi(x, t + \Delta t)\rangle = \left[e^{-i\frac{\hat{P}^2}{2m}\Delta t}e^{-iV(\hat{X})\Delta t} + O(\Delta t^2)\right]|\psi(x, t)\rangle. \quad (3)$$

For a sufficiently small time step  $\Delta t$ , Eq. (3) can be approximated as:

$$|\psi(x, t + \Delta t)\rangle = e^{-i\frac{\hat{P}^2}{2m}\Delta t}e^{-iV(\hat{X})\Delta t}|\psi(x, t)\rangle. \quad (4)$$

Similarly, the continuous degree of coordinate  $x$  is also discretized. Suppose  $\psi(x, t)$  is continuous on the region  $0 < x < L$ , with a periodic boundary condition

\*These authors make equal contribution to this work.

†Corresponding author, gllong@tsinghua.edu.cn

$\psi(x+L, t) = \psi(x, t)$ .  $x$  is discretized into a lattice with spacing  $\Delta l$  and the wave function is stored in an  $n$ -qubit quantum register

$$|\psi(x, t)\rangle \rightarrow \sum_{k=0}^{2^n-1} \psi(x_k, t) |k\rangle, \quad (5)$$

where  $x_k = (k + \frac{1}{2})\Delta l$ ,  $\Delta l = \frac{L}{2^n}$ , and  $|k\rangle$  is the lattice basis state corresponding to the binary representation of the number  $k$ . Apparently, Eq. (5) gives a good approximation to the wave function in the limit  $n \rightarrow \infty$ .

As a small-scale demonstration, a 2-qubit simulation is investigated. In this case, the four basis states  $|00\rangle$ ,  $|01\rangle$ ,  $|10\rangle$  and  $|11\rangle$  register the four lattice points 1, 2, 3 and 4 as discretized position variables of the particle.

Next we construct the kinetic and potential operators for the discretized wave function. Because the potential operator  $V(\hat{X})$  is a function of the coordinate operator  $\hat{X}$ , it is diagonal in the coordinate representation, though discretized now. In an  $n$ -qubit discretized grid,  $V$ , a diagonal matrix in the coordinate representation, can always be decomposed as

$$V = \sum_{i_1, i_2, \dots, i_n=3}^4 c_{i_1 i_2 \dots i_n} \otimes_{k=1}^n \sigma_{i_k}, \quad (6)$$

where each term in the summation corresponds to a diagonal entry with coefficient  $c_{i_1 i_2 \dots i_n}$ ,  $\sigma_3$  is the Pauli matrix  $\sigma_z = \begin{pmatrix} 1 & 0 \\ 0 & -1 \end{pmatrix}$ , and  $\sigma_4 = I$  is the identity matrix in two dimensions. One simple example of a potential for a 2-qubit system with the form of Eq. (6) is

$$V = V_0 I \otimes \sigma_z, \quad (7)$$

which corresponds to a double-well potential of amplitude  $2V_0$ , with the two peaks  $V_0$  at 00 and 10, and the two valleys  $-V_0$  at 01 and 11. This double-well potential can therefore be implemented using only a single qubit gate

$$Q = e^{-iV(\hat{X})\Delta t} = I \otimes e^{-iV_0\sigma_z\Delta t}. \quad (8)$$

Similar to Eq. (5), the wave function in the momentum representation can be written as

$$|\phi(p, t)\rangle \rightarrow \sum_{j=0}^{2^n-1} \phi(p_j, t) |j\rangle, \quad (9)$$

where

$$p_j = \begin{cases} \frac{2\pi}{2^n} j & 0 \leq j \leq 2^{n-1} \\ \frac{2\pi}{2^n} (2^{n-1} - j) & 2^{n-1} < j < 2^n \end{cases}$$

is the eigenvalue of the momentum operator  $\hat{P}_p$  (the subscript 'p' indicates the momentum representation) corresponding to the  $j$ -th basis  $|j\rangle$ . The momentum operator

is expressed in spectral decomposition form as

$$\hat{P}_p = \sum_{j=0}^{2^{n-1}-1} \frac{2\pi}{2^n} j |j\rangle \langle j| + \sum_{j=2^{n-1}+1}^{2^n-1} \frac{2\pi}{2^n} (2^{n-1}-j) |j\rangle \langle j| \quad (10)$$

Therefore the kinetic energy operator in the coordinate representation can be written via quantum Fourier transform (QFT) as

$$\frac{\hat{P}^2}{2m} = F^{-1} S^{-1} \frac{\hat{P}_p^2}{2m} S F, \quad (11)$$

where the QFT is expressed in terms of the bit swap gate  $S$ , and the bit-swapped quantum Fourier transform operator  $F$ .

For the 2-qubit system, Eq. (11) can be specifically expressed as

$$\frac{\hat{P}^2}{2m} = F^{-1} S^{-1} \frac{\pi^2}{4} \Pi S F, \quad (12)$$

where we have taken  $m = 1/2$ ,  $\Pi = (\text{diag}[0, 1, 2, -1])^2$ ,

$$S = \begin{pmatrix} 1 & 0 & 0 & 0 \\ 0 & 0 & 1 & 0 \\ 0 & 1 & 0 & 0 \\ 0 & 0 & 0 & 1 \end{pmatrix}$$

and

$$F = S^{-1} \frac{1}{2} \sum_{j,k=0}^3 e^{\frac{1}{2}i\pi jk} |j\rangle \langle k|. \quad (13)$$

$F$  can be readily implemented in quantum circuits via a series of Hadamard gates and controlled-phase gates [21]

$$F = H_2 R_{\frac{\pi}{2}} H_1, \quad (14)$$

where  $H_1$  and  $H_2$  are Hadamard gates on the first and second qubits, respectively, and  $R_{\frac{\pi}{2}} = \text{diag}[1, 1, 1, i]$  is the two-qubit controlled phase gate. The operator  $e^{-i\frac{\hat{P}^2}{2m}\Delta t}$  can be expressed as

$$e^{-i\frac{\hat{P}^2}{2m}\Delta t} = F^{-1} D F = F^{-1} \Phi_\pi Z_1 Z_2 F, \quad (15)$$

where

$$\Phi_\pi = \exp[-i\frac{3\pi^2}{4} R_\pi \Delta t], \quad (16)$$

$R_\pi = R_{\frac{\pi}{2}} R_{\frac{\pi}{2}}$  and

$$Z_1 = \exp[i\frac{\pi^2}{4} \sigma_z \otimes I \Delta t], \quad (17)$$

$$Z_2 = \exp[i\frac{3\pi^2}{4} I \otimes \sigma_z \Delta t]. \quad (18)$$

Operation  $\exp(-i(2\pi/4)^2 \text{diag}[0, 4, 1, 1] \Delta t)$  is realized through  $\Phi_\pi Z_1 Z_2$ , which is also a bit-swapped operator,

up to an overall phase factor. Thus the time-dependent Schrödinger Eq. (4) can be rewritten as

$$\sum_{k=0}^3 \psi(x_k, t + \Delta t) |k\rangle = F^{-1} \Phi_\pi Z_1 Z_2 F Q \sum_{k=0}^3 \psi(x_k, t) |k\rangle. \quad (19)$$

In the experiment, we studied the time evolution of a particle moving in a double-well potential in a digital algorithm in a 2-qubit system via the room temperature NMR system. A d6-acetone solution of  $^{13}\text{C}$ -labeled chloroform at 295K is used where  $^1\text{H}$  (with a resonance frequency 400.130 MHz) encodes the first qubit and  $^{13}\text{C}$  (with a resonance frequency 100.613 MHz) encodes the second qubit.

From Eq. (19) the one time step evolution quantum circuit for our simulation is straightforwardly obtained, as drawn in Fig. 1. The corresponding pulse sequences for implementing the operations in the quantum circuit are exhibited in Fig. 2.

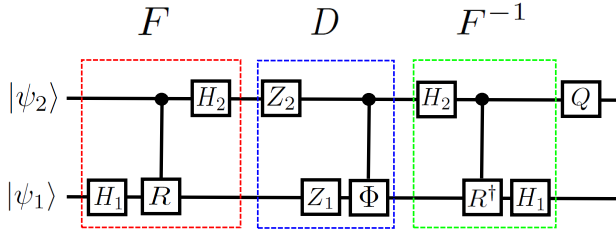


Figure 1: (Color online) Quantum circuit for one time step simulation.  $|\psi_1\rangle$  and  $|\psi_2\rangle$  are the input states of the first and the second qubit, respectively.

In our experiments we set the time interval to be  $\Delta t = \frac{1}{10}$  and the amplitude of the potential  $2V_0 = 20$ . We simulated the situation in which the particle is initially trapped inside one of the two wells by preparing the pseudo-pure state  $|01\rangle$  from the thermal equilibrium [22] as the initial state with an experimentally realized high fidelity  $f = 99.89\%$  (see Fig. 3) which is given by

$$f = \frac{\text{trace}(\rho_{ex} \rho_{th})}{\sqrt{\text{trace}(\rho_{ex}^2) \text{trace}(\rho_{th}^2)}} \quad (20)$$

where  $\rho_{th}$  is the theoretical density matrix, and  $\rho_{ex}$  is the experimental density matrix.

In order to observe the tunneling process of the particle, nine experiments have been carried out in which the pulse sequence in Fig. 2 has been performed 1 ~ 9 times. Quantum state tomography (QST) is performed on the density matrices of the final states after 1 to 8 steps ([23, 24]). The diagonal elements that correspond to the simulation of the probability distribution of the particle are illustrated in Fig. 6, compared with the theoretical results. The full density matrix of the final state after 9 steps in our experiment is shown fully in Fig. 4 along with the theoretical results. The fidelity of the experimental density is determined by Eq. (20) to be

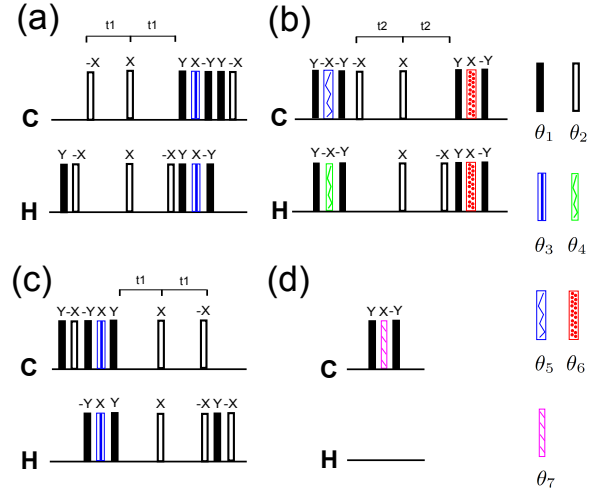


Figure 2: (Color online) Pulse sequences to implement the circuit in Fig. 1, where (a), (b), (c), (d) realize the four operations  $F$ ,  $D$ ,  $F^{-1}$  and  $Q$  respectively. The time periods  $t1 = \frac{1}{8J} = 580.9\mu\text{s}$  and  $t2 = \frac{\pi}{40J} = 365.0\mu\text{s}$  represent the free evolution durations under the  $J$  coupling (for chloroform  $J = 215.2\text{Hz}$ ). The bars represent single-qubit rotation pulses with the different angles as shown to the right, and seven different fillings indicate different rotation angles as  $\theta_1 = \frac{\pi}{2}$ ,  $\theta_2 = \pi$ ,  $\theta_3 = \frac{\pi}{4}$ ,  $\theta_4 = \frac{\pi^2}{40}$ ,  $\theta_5 = \frac{\pi^2}{10}$ ,  $\theta_6 = \frac{\pi^2}{20}$ ,  $\theta_7 = 2$ , respectively.

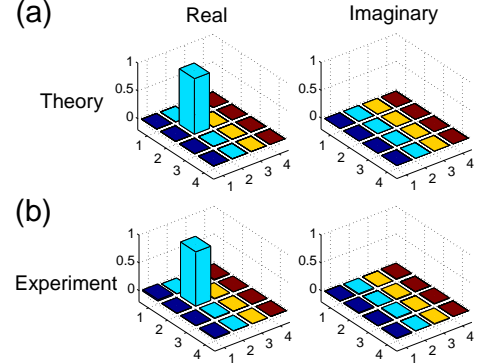


Figure 3: (Color online). The real and imaginary parts of (a) the density matrix of the  $|01\rangle$  state; (b) the density matrix reconstructed by QST for the initial  $|01\rangle$  state in our experiment.

95.48%. As is depicted in Fig. 6 (b), the whole evolution process of a single particle's probability distribution in the double-well potential can be obtained through our 9-step experiment. It can be clearly observed that the particle tunnels through the potential barrier between the two wells, while its probability to be found in the barrier is scarce, which accords well with the theoretical calculations in Fig. 6 (a).

For the sake of comparison we also studied the simulation of the evolution of a free particle with zero potential

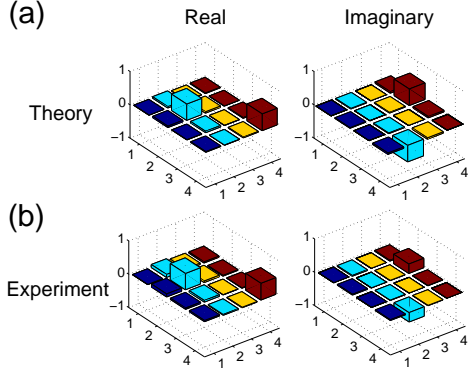


Figure 4: (Color online). The real and imaginary parts of (a) the theoretically calculated density matrix after nine steps of evolution in a double well potential; (b) the experimental density matrix reconstructed by QST after the nine steps of evolution in a double well potential.

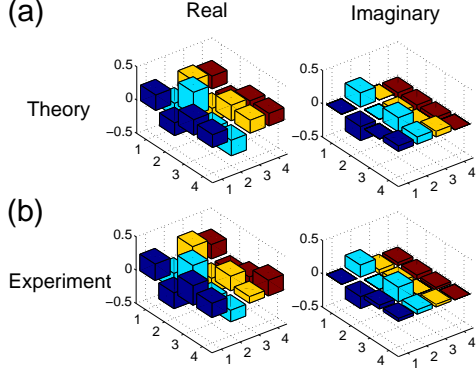


Figure 5: (Color online). The real and imaginary parts of (a) the theoretically calculated density matrix after nine steps of evolution without double well potential; (b) the experimental density matrix reconstructed by QST after nine steps of evolution without the double well potential.

using approximately the same experimental schemes and parameters, except for the removal of the potential operator  $Q$  in the circuit, and its corresponding RF pulse sequences were also performed from one to nine times. The final state reconstructed by full QST is shown in Fig. 5 with a fidelity of 96.82% according to Eq. (20). The results of these nine experiments, together with the theoretical calculations, are plotted in Fig. 7 to illustrate the evolution of a free particle. It is not surprising to find that the probability distributed more evenly on all the four lattice points, considering the particle is free.

Our experiments have simulated the fundamental quantum phenomenon of tunneling and reflected an evidential difference between the two situations with and without the double-well potential. If more qubits are used in the simulation, more specific dynamic phenom-

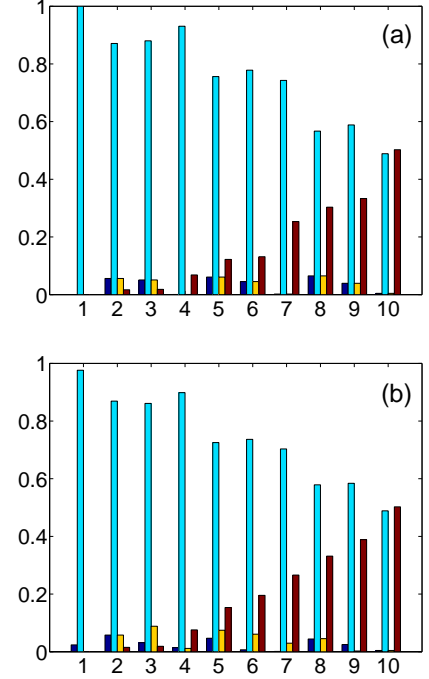


Figure 6: (Color online). A single particle's probability distributions as a function of time for the first nine steps for a particle in a double well potential. The two potential wells are at  $|01\rangle$  (lattice point 2) and  $|11\rangle$  (lattice point 4). (a) The theoretical predictions; (b) The liquid NMR experimental results. The four bars (from left to right) at each step indicates the particle's probability on the state  $|00\rangle$  (blue),  $|01\rangle$  (green),  $|10\rangle$  (yellow),  $|11\rangle$  (red), from left to right. The initial state is prepared in  $|01\rangle$ . As is illustrated in (a) and (b), the particle tunnels from  $|01\rangle$  to  $|11\rangle$ . Our experiments agree quite well with theoretical results depicted, clearly manifesting the tunneling phenomenon.

ena of quantum tunneling can be observed, for example, with higher position resolution in wells or in barriers, the oscillation of the state in wells or in barriers can be observed. An  $N$ -lattice-point simulation can be realized with only  $\log_2 N$  qubits, which means the scheme is efficient and easily implemented in experiments. The experimental realization of multi-qubit simulation of quantum tunneling will be studied in our future work.

It should be emphasized here that although the real evolution of the particle takes place in a continuous space with infinite dimensions, the quantum computer, via only a few qubits with limited dimensions (in our case four dimensions), is already capable of undertaking some basic yet fundamental simulation tasks, such as quantum tunneling. The result has revealed the amazing power hidden under the qubits and the promising future of quantum computations.

In summary, we accomplished a small-scale demonstration of the quantum tunneling process on the 2-qubit NMR system based on the digital quantum simulation method. To our knowledge this is the first demonstra-

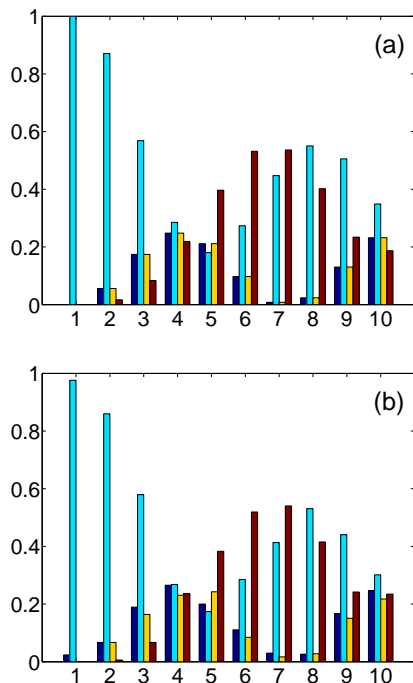


Figure 7: (Color online). The free particle's probability distributions as a function of time for the first nine steps. (a) The theoretical predictions; (b) The liquid NMR experimental results. The four bars at each step indicates the particle's probability on the state  $|00\rangle$  (blue),  $|01\rangle$  (green),  $|10\rangle$  (yellow),  $|11\rangle$  (red), from left to right. The initial state is prepared to be  $|01\rangle$ . As is illustrated in (a) and (b), the particle's probability becomes more evenly distributed among all the four states. Our experiments agree quite well with theoretical results depicted.

tion work on quantum tunneling simulations via an NMR quantum information processor. The experimental results and the theoretical predictions are in agreement. The overlaps of the final states after nine steps of evolution (with and without the double-well potential) between the experimental results and the theoretical predictions are about 95%, which manifests the high quality of the experimental results.

This work was supported by the National Natural Science Foundation of China under Grant No. 11175094, the National Basic Research Program of China under Grant Nos. 2009CB929402 and 2011CB9216002, and the SRFDP under Grant No. 20110002110007.

- 
- [1] Richard P. Feynman, International Journal of theoretical Physics 21, 467(1982).
  - [2] E. Gerjuoy, Am. J. Phys. 73, 521-540 (2005).
  - [3] L. K. Grover, Rhys. Rev. Lett. 79, 325(1997).
  - [4] C.H. Tseng, S. Somaroo, Y. Sharf, E. Knill, R. Laflamme, T.F. Havel and D.G. Cory, Phys. Rev. A 61, 012302(1999).
  - [5] C. Negrevergne, R. Somma, G. Ortiz, E. Knill and R. Laflamme, Phys. Rev. A 71, 032344(2005).
  - [6] X.H. Peng, J.F. Zhang, J.F. Du and D. Suter, Phys. Rev. Lett. 103, 140501(2009).
  - [7] J.F. Zhang, T.-C. Wei and R. Laflamme, Phys. Rev. Lett. 107, 010501(2011).
  - [8] X.H. Peng, J.F. Du and D. Suter, Phys. Rev. A 71, 012307(2005).
  - [9] E.E. Edwards, S. Korenblit, K. Kim, R. Islam, M.- S. Chang, J.K. Freericks, G.-D. Lin, L.-M. Duan and C. Monroe, Phys. Rev. B 82, 060412(2010).
  - [10] J.F. Zhang, F. M. Cucchietti, C. M. Chandrashekar, M. Laforest, C. A. Ryan, M. Ditty, A. Hubbard, J. K. Gamble, and R. Laflamme, Phys. Rev. A 79, 012305(2009).
  - [11] B.P. Lanyon, J.D. Whitfield, G.G. Gillett, M.E. Goggin, M.P. Almeida, I. Kassal, J.D. Biamonte, M. Mohseni, B.J. Powell, M. Barbieri, A. Aspuru-Guzik and A.G. White, Nature Chemistry 2, 106111(2010).
  - [12] J.F. Du, N.Y. Xu, X.H. Peng, P.F. Wang, S.F. Wu and D.W. Lu, Phys. Rev. Lett. 104, 030502(2010).
  - [13] I. Kassal, J.D. Whitfield, A. Perdomo-Ortiz, M.-H. Yung and A. Aspuru-Guzik, Annu. Rev. Phys. Chem. 62, 185(2011).
  - [14] I. Kassal, S.P. Jordan, P.J. Love, M. Mohseni and A. Aspuru-Guzik, Proc. Nat. Acad. Sci. USA 105, 18681(2008).
  - [15] B. D. Josephson, Phys. Lett. 1, 251 (1962).
  - [16] Leo Esaki and Yuriko Miyahara, Solid-State Electronics 1, 13(1960).
  - [17] G. Binnig and H. Rohrer, IBM Journal of Reserch and Development 44, 279-293(2000).
  - [18] Andrew T. Sornborger, arXiv:1202.1536v1 (2012). In our work, we exchanged the  $c_0$  in  $Z_0$  with  $c_1$  in  $Z_1$ .
  - [19] C. Zalka, Proc. R. Soc. Lond. A 454, 313(1998).
  - [20] G. Benenti and G. Strini, Am. J. Phys. 76, 657(2008).
  - [21] D. Coppersmith, IBM Research Report, RC19642(1994).
  - [22] David G. Cory, Mark D. Price and Timothy F. Havel,

- Physica D: Nonlinear Phenomena 120, 82 (1998). Semiclass. Opt. 3, 376 (2001).
- [23] Jae-Seung Lee, Phys. Lett. A 305, 349(2002).
- [24] G L Long, H Y Yan and Y Sun, J. Opt. B: Quantum